A fast three-dimensional deterministic ray tracing coverage simulator for a 24 GHz anti-collision radar

H. Azodi, U. Siart, and T. F. Eibert

Lehrstuhl für Hochfrequenztechnik, Technische Universität München, Arcisstr. 21, 80333 Munich, Germany

Correspondence to: H. Azodi (hossein.azodi@tum.de)

Abstract. A matrix-based approach for implementation of deterministic ray tracing is suggested and presented in this paper. The frequency-independent feature of the ray tracing in addition to the matrix-based implementation results in a reliable fast simulator for understanding the behavior of the electromagnetic fields in the vicinity of a collision avoidance radar. Results of this technique are in a good agreement with the results from method of moments integral equation solutions while the computations are about 100 times faster.

1 Introduction

Computer numerical control (CNC) machines are a group of manually programmed modern machines for drilling, milling, laser or plasma cutting, etc. (Fig. 1). They are ranged within the expensive workshop machinery. Due to human errors in coding their controls, disastrous collisions between the tool of the machine and surrounding metallic objects can easily cause very expensive damage. It is, therefore, wise to detect possible collisions in advance and stop the machine. For this reason, we suggest to encircle the tool of CNC machines with a number of radar modules to detect the possibility of harmful collisions and to stop the machine before collisions take place.

Figure 2 shows a mock-up of CNC tool and the radar modules surrounding it. We propose to use the minimum of 3 modules with 120° circular distance so that full coverage of the surrounding space can be achieved. Thanks to the simple and symmetrical geometry any calculation or simulation for one module can be easily expanded for other modules in different positions. The radiator of this module is a linear patch array antenna with 8 elements which operate in the ISM band around 24.125 GHz.

Due to frequent replacements of tool, object, etc., a CNC machine has a varying electromagnetic environment. Conse-

quently, the radar system requires to calibrate itself throughout the operational mode of the machine. On the other hand, the design should remain consistent and practically compatible with any CNC machine. These highly-demanding features require an accurate, fast, and reliable radar system. False alarms, not desirable though, are accepted but collision detection failure is not permitted at all.

From an electromagnetic point of view, this problem can be categorized in near-field antenna propagation modeling and channel estimation. Understanding the behavior of electromagnetic (EM) waves in the vicinity of the tool plays the most important role in designing such a radar system. In the next section, we explain why ray tracing is a good candidate for simulating the fields and obtaining the channel model. In Sect. 3, the main idea of our fast deterministic ray tracing approach is explained and the results of this approach are presented in Sect. 4. Section 5 concludes this paper.

2 Electromagnetic modeling and solution technique

The mock-up, which contains the most important characteristics of the tool of the CNC machine, is modeled with two cylinders (Fig. 3). The antenna is located on the holder. As shown in Fig. 4, a single patch array antenna in an open PEC cavity is used. The electromagnetic modeling of the antenna itself and its local environment is decoupled from the propagation problem. The current electromagnetic model includes the most important aspects of the mock-up. A detailed model is simply created by adding more cylinders to the model. Therefore, we sticked to this simple model at this stage and for later stages we will add more complexities to the model. It is, indeed, possible due to flexibility of our simulation technique which becomes evident to the readers in the rest.

Finite Difference Time Domain (FDTD), Integral Equation (IE) and Ray Tracing are 3 candidates to simulate the fields of the electromagnetic wave propagation problem.

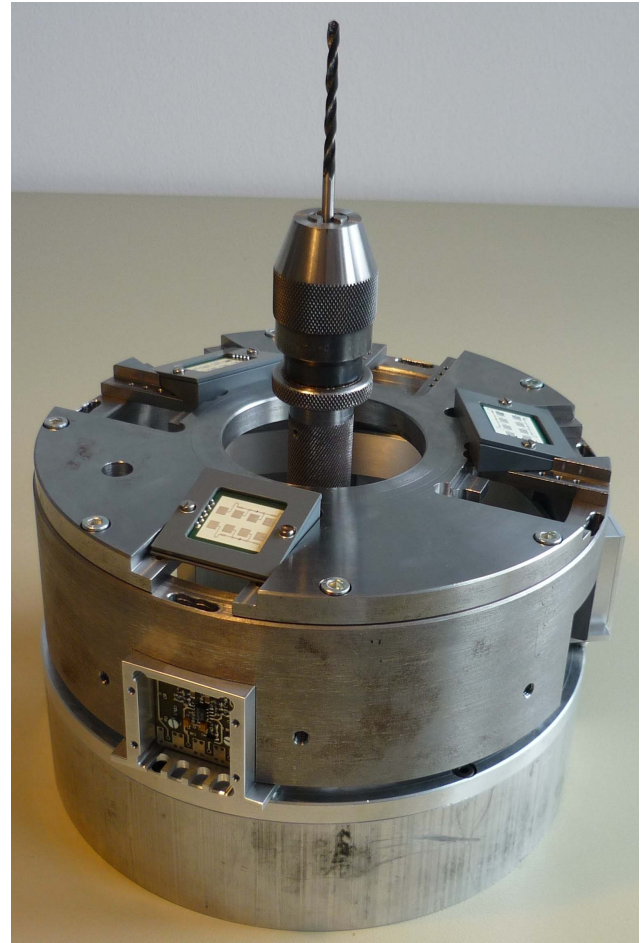**Fig. 1.** Tool of a CNC and its machinery

Fig. 2. Initiative measurement mock-up designed and manufactured in our workshop and the Radar module on the surrounding area

A typical FDTD code would need more than $10 \, \text{lines}/\lambda$ at $F_{\text{CEN}} = 24 \, \text{GHz}$ leads to 38 million mesh-cells for the structure which takes several days of CPU time for every scenario on a quad-core computer with $12 \, \text{GB}$ of RAM. Moreover, 10 lines per wavelength is the minimum and for more accurate results an increase to $16 \, \text{lines}/\lambda$ is recommended. Consequently, simulations at higher ISM bands such as $F_{\text{CEN}} = 60 \, \text{GHz}$ appear impractical.

The Method of Moments (MoM) – integral equation (IE) method is another potential solution candidate, particularly suitable due to the fully metallic surface of the geometry. The problem can therefore be discretized with about 5 million unknowns at $24 \, \text{GHz}$. This can be handled with the aforementioned computer, although it is a big problem. Hence, the IE method is used as a standard method to compare and validate the results of the ray tracer as it is still a big problem for every-day optimization and design processes. For this purpose, an in-house IE-MoM code is used Eibert (2004).

The third candidate to solve this problem is ray tracing Ling et al. (1989). As mentioned in Sect. 1, this is a near-field problem. In contrary, ray tracing is a method where fields

are assumed to propagate in the far-field region. This is the estimation which should be taken into account in order to achieve the benefits of ray tracing method. This estimation can be improved by considering more geometrical details of the objects such as curvature, multiple reflections, etc. In our approach the problem of antenna simulation and field calculations are decoupled. The antenna far-field pattern is obtained using FDTD technique and it is inserted into the wave propagation ray tracing code. Once the ray paths to an observation point is found, field calculation is a summation of the initial fields of antenna pattern multiplied by reflection or diffraction coefficients depends on path, free space loss and propagation phase shift.

In Shooting and Bouncing Rays (SBR) Ling et al. (1989), millions of rays are launched from the transmitter. The path of the ray is traced until reaching the observation point or leaving the simulation bounds. Even in an indoor scenario a very small portion of the rays will reach observation points. So, calculating paths of such a huge number of rays wastes resources in case one could anticipate the potential paths.
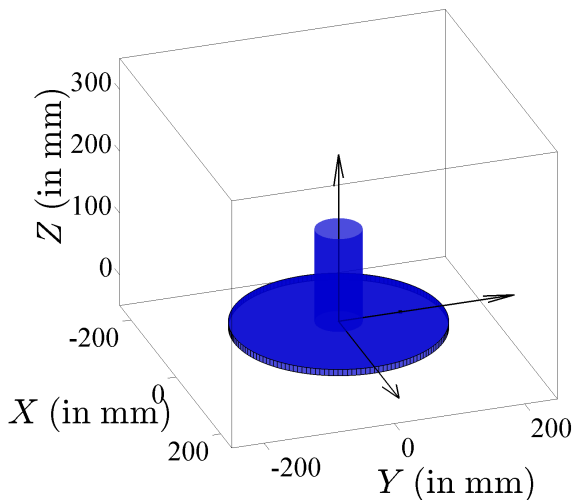
Fig. 3. Electromagnetic modeling of the initiative mock-up. The problem is decoupled in modeling the geometrical scenario and antenna, separately.

This will bring the idea of deterministic ray tracing while we have a priori information by knowing the geometry of the problem.

Another problem arises in SBR when a ray closely passes the observation point. As an observation point is theoretically dimensionless, these rays are usually not included. Nevertheless, it is seen that Flores et al. (1998); Noori et al. (2006) these missing rays might have an effect on the field of that point. Therefore, the idea of reception sphere is developed as a solution to this problem. In our deterministic ray tracing method, the observation point and all the other points remain dimensionless, i.e. ideal, and we are still able to calculate reaching paths to them accurately.

3   Fast matrix-based deterministic ray tracing

Deterministic ray tracing is suggested and developed in order to obtain the EM fields in the vicinity of the radar. This method enables us to have an overview of the coverage of the radiation strength and to estimate the channel response much faster than the aforementioned discretizing methods. As calculations are done using *same-size* matrices, a loopless MATLAB® code will provides with the results in a few minutes on the used PC.

From a general perspective, the idea of matrix-based deterministic ray tracing consists of two main parts. In the first part, the code calculates the required (mostly) geometrical matrices and the second part of the code is responsible for calculating the fields due the various rays and adding them together. These two parts are explained in Sects. 3.1 and 3.2, respectively.
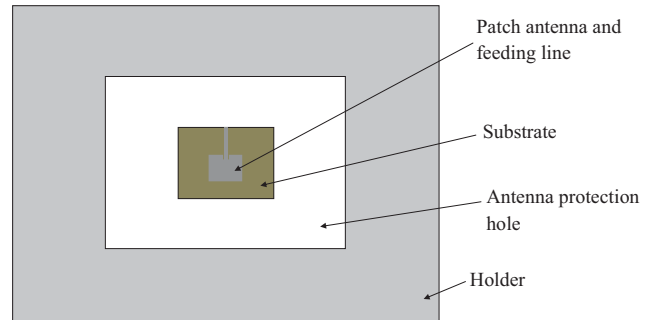

Fig. 4. Modeling of antenna as a single patch in a box of PEC. The box is empty and the antenna is a single patch fed with microstripline.

3.1   Pre-calculation and matrix formation

The entire observation space is discretized with equi-distant grids. For each grid in the observation space, there exists a unique element in every matrix. For example, $\mathbf{X} = [x_{mnp}]$ is the X-coordinate of the grid in the position of (m, n, p) of the space. The same applies to $\mathbf{Y}$ and $\mathbf{Z}$ matrices. Size of the matrices depends on the discretization fineness. The complexity of the problem increases with resolution as well but not with frequency.

Having these matrices, the rest of the pre-calculation phase is determining the geometrical matrices. For instance, the Euclidean distance to the origin:

$$\mathbf{R} = \left[\sqrt{x_{mnp}^2 + y_{mnp}^2 + z_{mnp}^2} \right] \tag{1}$$

where all operations are element-wise. Equation (1) can be implemented in MATLAB® without using a loop. Any other required matrix can be calculated with the same principle.

The most important matrices in the pre-calculation phase are *shadow (or illumination)* matrices. Zero, 0, in a shadow (or one, 1, in an illumination) matrix means the corresponding observation point, P_{mnp}, is illuminated, counterpart means it is shadowed. Obviously, shadow matrices are ray dependent. These matrices contain the information of ray paths. So, in computation of them the Fermat's principle is used. This means, for example, for the direct ray the direct path from the antenna to the observation point is considered.

To calculate these matrices numerically, a geometry data matrix, $\mathbf{B}_{\text{GEO}}$, is created first. One, 1, in $\mathbf{B}_{\text{GEO}}$ indicates that the corresponding point in the space is occupied with an object (or a part of an object). For empty space the matrix returns 0. Thus, the size of this matrix is the same as other matrices and if higher accuracy is required, finer discretization can be applied. The shadow matrix element for the observation point (m, n, p) is, therefore,

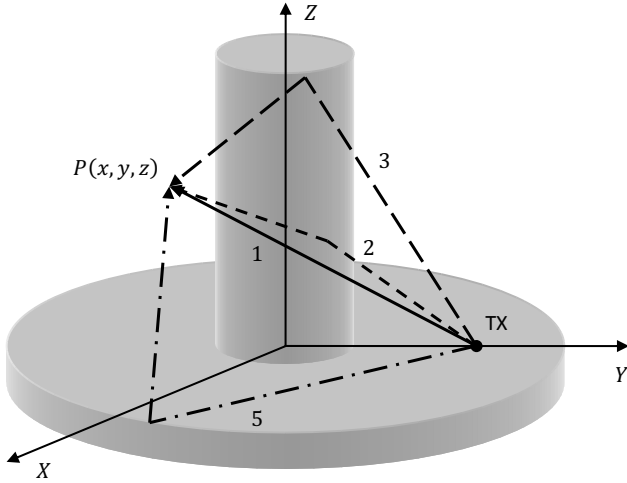$$s_{mnp} = \left(\int_{T_{mnp}}^{P_{mnp}} \mathbf{B}_{\text{GEO}} \, \mathrm{d}l \geq 1 \right) \tag{2}$$

Fig. 5. 5 rays contribute to find out the field in one point. They are identified with numbers on each path. As creeping ray and direct ray cannot reach an observation point together, in this schematic the chosen point is not illuminated by creeping ray.

Fig. 6. Magnitude of E-field in surrounding space of the machine sliced every 45 degrees.

where T_{mnp} is the position of the transmitter corresponding to the observation point at P_{mnp} and the ray type. It should be noted again that depending on the ray type the transmitter position can be different from the antenna position. For instance in reflection from the cylinder, the transmitter is first the antenna but, later, when we need the path from the reflection point to the observation point, it becomes a point on the cylinder. The reflection point is computed based on Fermat's principle and is saved in the corresponding element of the "reflection point from the cylinder" matrix. The integral in Eq. (2) is over the connecting straight line between the points T_{mnp} and P_{mnp} and the integrand is the geometry data function of the space. By discretization,

$$s_{mnp} = \left(\sum_i [b_{m_i n_i p_i}] \geq 1 \right) \tag{3}$$

where $[b_{m_i n_i p_i}]$ runs over the elements of geometry data matrix which fall in the connecting line of transmitter and observation points. Calculating all s_{mnp}, the shadow matrix, $\mathbf{S} = [s_{mnp}]$, is created.

The pre-calculation process is finished by calculating the geometrical matrices, shadow (or illumination) matrices and incident field matrices. Incident field matrices correspond to amplitude and phase of the fields which are just propagated in the direction of the ray path from the antenna. These fields are generated by interpolating the spherical coordinates of the direction and the far-field pattern.
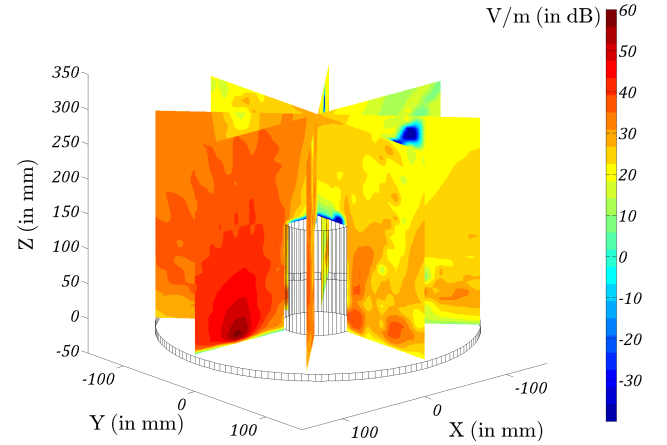
Contributions of 5 rays are summed up in our simulations. These rays are direct ray, reflected ray by the cylinder, diffracted ray by the upper edge of cylinder, creeping ray around the cylinder, and diffracted ray by the edge of the holder (Fig. 5).

3.2 Field calculation and summation

Except the direct path from the transmitted to the observation point, the other paths are going through several points on the structure. The coordinates of these points in each ray type are calculated and stored in separate matrices. For example for the reflection from the cylinder, there is a point on the cylinder where the reflection occurs, obviously. The coordinates of this point are stored in $\mathbf{X}_{N,REF}$, $\mathbf{Y}_{N,REF}$, and $\mathbf{Z}_{N,REF}$, respectively. It should be noted again that the elements of matrices are in accordance with the observation point. This means that $\mathbf{X}_{N,REF} = [x_{mnp}]$ has the first coordinate of the point N_{REF} in accordance with the observation point P_{mnp}. N_{REF} can be computed using the geometrical optics rule of reflection. Taking into account that N_{REF} is a point on the cylinder with, i.e. $0 \leq z_{mnp} \leq H_{CYL}$ and $x_{mnp}^2 + y_{mnp}^2 = R_{CYL}^2$, where H_{CYL} and R_{CYL} are height and radius of the cylinder, respectively, a quadratic equation is obtained which in principle has 4 roots. From them, only one is the desired root for P_{mnp}. This root is real and belongs to the illuminated side of the cylinder. Thus, a direct solution Tignol (2004) to the equation will provide us with the desirable result.

For the diffraction from the holder cylinder (the second cylinder), where the grazing rays of the antenna approaches the circular edge of the cylinder, the story is quite different. The geometrical equation is a non-linear trigonometric equation from degree of 6. Consequently, there are more than one point from which a path to the observation point, P_{mnp}, exists. In order to consider all the diffraction points on the
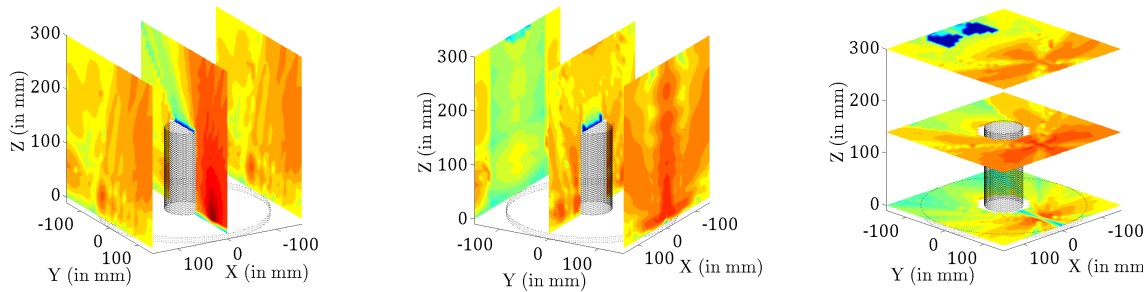
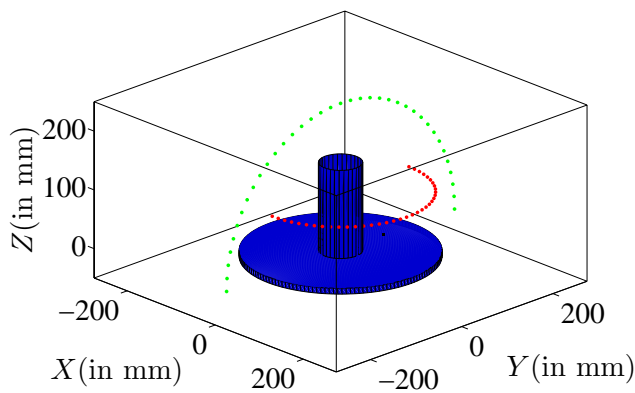**Fig. 7.** Magnitude of E-field in surrounding space of the machine sliced w.r.t. X-, Y-, and Z-axes.

Fig. 8. Point series positions to compare the result of deterministic ray tracing and MoM-IE technique.

holder edge, the code finds 5 roots of about 30 000 equations simultaneously. Number of equations comes directly from the number of observation points for which the field is computed. It depends on the desired fineness of computation domain. The maximum number of roots (5 in this case) is only the maximum real roots of any equation. In order to have an efficient method regarding the computation time, it is necessary to solve all these equations and to retrieve their zeros simultaneously. Otherwise, our technique takes the same time as stochastic ray tracing techniques. To the best understanding of the authors, the iterative algorithm in Ying and Katz (1989) is the most reliable and general algorithm to find out the multiple roots of an equation. This algorithm is expanded in our code to solve the equations in matrix form, i.e. 30 000 equations altogether.

Creeping rays (James, 1986, Pages 195–203) are also taken into account to uniform the transition from illuminated to deep shadow region. On the cylinder, a creeping ray follows a geodesic path which is simply a helical curve. The characteristics of the helical path is subjected to geometrical ray optics with the condition that on the starting and ending parts the ray is tangent to the cylinder.

Finding the paths, the field in every observation point can be obtained. The antenna is simulated separately where it is buried in body of PEC and covered by a dielectric material

with relative permittivity close to 1 (Fig. 4). The far-field pattern of the antenna is stored in a file so that for every direction of Θ and Φ in the space the amplitude and phase of the incident field is known. As our observation points do not fall exactly on the saved directions of the far-field pattern, we interpolate this file with the point directions to calculate the incident fields. Later, they are multiplied by the coefficients of that path, e.g. reflection or diffraction coefficients (James, 1986, Page 233) for reflection from the cylinder or diffraction from the edge of the cylinder, respectively, and so on. These coefficients have the effect of the astigmatic loss included. Each path, additionally, has its own propagation phase term which is also multiplied. Finally, the field matrix due to each ray is filtered by the corresponding illumination matrix. As the result, fields become null in shadowed points and when they are summed up, the result has the contributions of the physically reachable rays to that point.

4   Results

The deterministic ray tracer code is used to simulate the surrounding space of the radar system in $31 \times 31 \times 31 = 29\,791$ equi-distant grids in the single center frequency of $F_{\mathrm{CEN}} = 24.145\,\mathrm{GHz}$. This simulation covers the space within the range of $-150\,\mathrm{mm}$ to $150\,\mathrm{mm}$ for X or Y and $0\,\mathrm{mm}$ to $300\,\mathrm{mm}$ for Z. The entire simulation process takes $42\,\mathrm{min}$ while this is almost the same time it takes for a C/C++ shooting and bouncing ray tracer to deliver the result of a single transmitter and single receiver scenario. The computer has a $2.67\,\mathrm{GHz}$ quad-core i7 Intel® CPU and is running Win 7 64 bit with $12\,\mathrm{GB}$ of RAM.

Figure 6 presents the magnitude of E-field in logarithmic scale. In this figure, fields are sliced every $\Delta\Phi = \pi/4$. The same scaling is used for the field magnitudes in Fig. 7. The magnitude of the fields in this figure are presented in different layers along the principal coordinate axes. The antenna is located at $(X, Y, Z) = (0, 95, 0)$ mm.

In another experiment, the result of deterministic ray tracer is compared with the result of MoM-IE technique. For this purpose, we used the calculation method of Eibert (2004) to simulate the fields in 2 series of points in Fig. 8. The
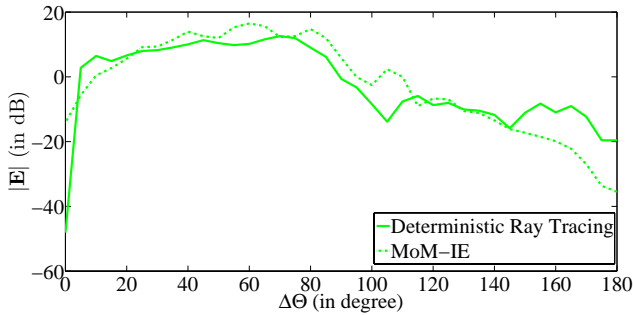
Fig. 9. Comparing the Ray Tracing and MoM-IE at the position of the green points in Fig. 8.
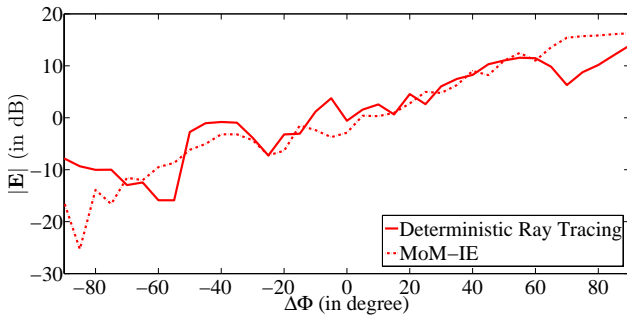

Fig. 10. Comparing the Ray Tracing and MoM-IE at the position of the red points in Fig. 8.

green points are located in the upper half-plane of $Y = 0$ in every 5 degrees on a circle with the radius of 250 mm and center of $(X, Y, Z) = (0, 0, 0)$. The red points are located in $Z = 100$ mm plane on a half circle with radius of 150 mm and center of $(X, Y, Z) = (0, 0, 100)$. The result of this comparison is presented in Figs. 9 and 10.

Comparing in both cases shows that the result of ray tracing stays in a good agreement with MoM-IE technique in the illumination and transition regions. In deep shadow region, ray tracer does not follow the same trend which results up to 10 dB difference. Higher accuracies are achievable by adding more details in the cost of higher runtime. In our application, we need a fast qualitative field distribution in an electrically large area. In this respect, the code performs well by computation of the electrical field in about 30 000 points which cover the surrounding space. This runtime will increase linearly with number of rays. However, the runtime does not depend on fineness of the geometry matrix. The latter feature is very helpful to increase the accuracy of computation.

5   Conclusions

In this work, a fast deterministic ray tracer technique with matrix-based approach was presented. It was coded for a simple geometry scenario, however, the main functions such as the simultaneous multiple root finder and shadow region detector are in their most general forms. This means with a priori knowledge of the number of needed rays, one may simulate the EM fields for any structure as the structure can be imported with a simple geometry boolean data matrix. Based on the simulation, one not only may investigate coverage but also calculate the channel impulse response complete Doppler or FMCW radar scenarios. The most important advantage of the code is the frequency-independent short time of computation which is needed for complex scenarios and scenarios including moving targets where many simulations should be carried out.

References

Eibert, T.: Iterative-Solver Convergence For Loop-Star And Loop-Tree Decompositions in Method-of-Moments Solutions of the Electric-Field Integral Equation, IEEE Antenn. Propag. M., 46, 80–85, doi:10.1109/MAP.2004.1374101, 2004.

Flores, S., Mayorgas, L., and Jimenez, F.: Reception Algorithms For Ray Launching Modeling of Indoor Propagation, in: Proceedings of IEEE Radio and Wireless Conference, 261–264, 1998.

James, G. L.: Geometrical Theory of Diffraction For Electromagnetic Waves, 3rd Edn., IET, 1986.

Ling, H., Chou, R.-C., and Lee, S.-W.: Shooting and Bouncing Rays: Calculating the RCS of an Arbitrarily Shaped Cavity, IEEE T. Antenn. Propag., 37, 194–205, 1989.

Noori, N., Shishegar, A., and Jedari, E.: A New Double Counting Cancellation Technique For Three-Dimensional Ray Launching Method, in: IEEE Antennas and Propagation Society International Symposium, 2185–2188, 2006.

Tignol, J.-P.: Galois' Theory of Algebraic Equations, 2nd Edn., World Scientific Publisher Co., 2004.

Ying, X. and Katz, I.: A Simple Reliable Solver For All the Roots of a Nonlinear Function in a Given Domain, Computing, 41, 317–333, 1989.